

# Surface modification of Ag<sub>3</sub>PO<sub>4</sub> using the alginate for highly active photocatalyst under visible light irradiation

*by Admin Publikasi*

---

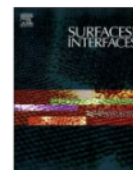
**Submission date:** 27-Mar-2022 02:57PM (UTC+0700)

**Submission ID:** 1793837862

**File name:** Surfaces\_and\_Interfaces-Surface\_modification\_kompress.pdf (858.03K)

**Word count:** 7807

**Character count:** 40967



# Surface modification of $\text{Ag}_3\text{PO}_4$ using the alginate for highly active photocatalyst under visible light irradiation

Uyi Sulaeman<sup>a,\*</sup>, Yusvirza Khairullah Gandasasmita<sup>a</sup>, Hartiwi Diastuti<sup>a</sup>, Ponco Iswanto<sup>a</sup>,  
Isnaeni Isnaeni<sup>b</sup>, Ardiansyah Taufik<sup>c</sup>, Shu Yin<sup>c</sup>

<sup>a</sup> Department of Chemistry, Jenderal Soedirman University, Purwokerto 53123, Indonesia

<sup>b</sup> Research Center for Physics, Indonesian Institute of Sciences, Building 442 Puspiptek, South Tangerang, Banten 15314, Indonesia

<sup>c</sup> Institute of Multidisciplinary Research for Advanced Materials, Tohoku University, Sendai 980-8577, Japan

## ARTICLE INFO

### Keywords:

$\text{Ag}_3\text{PO}_4$   
Alginate  
Chemisorption  
Conjugate  
Photocatalyst

## ABSTRACT

Surface modification of  $\text{Ag}_3\text{PO}_4$  using alginate has been successfully synthesized.  $\text{Ag}_3\text{PO}_4$  was prepared by precipitation method using  $\text{CaHPO}_4$ /hydroxyapatite composite as a source of phosphate ion and  $\text{AgNO}_3$  ethanol solution. Alginate was introduced on the surface of  $\text{Ag}_3\text{PO}_4$  under the chemisorption method. Products were analyzed using XRD, DRS, PL spectra, FTIR, SEM, TEM, and XPS. A small band edge absorption at 729 nm was created after surface modification using alginate. XPS analysis showed that the binding energy shifts of 0.3 eV and 0.5 eV were observed after alginate treatment for Ag3d and P2p respectively indicating that the alginate was successfully chemically bound to the  $\text{Ag}_3\text{PO}_4$  surface. The alginate-modified  $\text{Ag}_3\text{PO}_4$  photocatalyst showed much higher photocatalytic activity than pure  $\text{Ag}_3\text{PO}_4$ . The high activity is caused by the formation of conjugates that can act as electron donors under visible light irradiation.

## 1. Introduction

The development of  $\text{Ag}_3\text{PO}_4$  photocatalyst is very rapid for a decade due to owing high activity under visible light exposure. The most interesting in the development of  $\text{Ag}_3\text{PO}_4$ -based photocatalysts is the surface modification through an incorporating of elements and functional group of compounds that could improve the activity and stability of photocatalyst. This modification is very simple, cheaper, and has great challenges to provide an excellent photocatalyst.

The surface modification of  $\text{Ag}_3\text{PO}_4$  photocatalyst can utilize an inorganic and polymer compound. The modification using inorganic compounds of ammonium phosphate [1], copper [2], tungsten [3], platinum complexes [4], and ionic liquid [5] has successfully improved the properties of  $\text{Ag}_3\text{PO}_4$ . An ammonium phosphate can be utilized for  $\text{Ag}_3\text{PO}_4$  surface modification resulting in a much higher photocatalytic performance for organic dye degradation under visible light irradiation [1]. Ammonium ion etching leads to a surface transition from  $\text{Ag}_3\text{PO}_4$  to  $\text{Ag}^0$  producing higher capture of photogenerated electrons, generating much higher  $\bullet\text{O}_2^-$  radicals, whereas the adsorbed  $\text{PO}_4^{3-}$  on the  $\text{Ag}_3\text{PO}_4$  surfaces lead to more a negative electrostatic field which enhances the holes flowing to the surface, generating much higher  $\bullet\text{OH}$  radicals. The

band-gap energy of  $\text{Ag}_3\text{PO}_4$  can also be modified using Cu under the sol-gel method [2]. The shift of the bandgap from 2.07 to 1.00 eV leads to higher activity under visible light irradiation. The incorporating tungsten (W) in  $\text{Ag}_3\text{PO}_4$  was also successfully synthesized using the facile chemical precipitation method [3]. The  $\text{W}^{6+}$  can replace the  $\text{P}^{+x002B5}$  in form of  $\text{WO}_4^{2-}$ . This approach is similar to modification using platinum complexes, where  $\text{PO}_4^{2-}$  can easily be substituted by  $\text{PtCl}_6^{2-}$  on the surface [4]. These phenomena improve catalytic activity. The ionic liquid can also be utilized to modify the surface of  $\text{Ag}_3\text{PO}_4$ . The ionic liquid of 1-butyl-3-methylimidazole dihydrogen phosphate can increase the facet of {111} in  $\text{Ag}_3\text{PO}_4$  surface leading to higher catalytic activity [5].

Many designs of highly active photocatalysts are organic polymers incorporated on the  $\text{Ag}_3\text{PO}_4$  surface. The modification of  $\text{Ag}_3\text{PO}_4$  using cyclized polyacrylonitrile (CPAN) improved the photocatalytic ability under visible light irradiation [6]. This higher activity was due to generating  $\text{h}^+$  in the valence band of  $\text{Ag}_3\text{PO}_4$  and  $\bullet\text{O}_2^-$  radicals in the conduction band of CPAN. The polypyrrole (PPy) and multi-walled carbon nanotubes (MWCNTs) were successfully incorporated on the surface of  $\text{Ag}_3\text{PO}_4$  [7]. This modification can bring the photogenerated holes can easily migrate to the surface of PPy, whereas the

\* Corresponding author.

E-mail address: [sulaeman@unsoed.ac.id](mailto:sulaeman@unsoed.ac.id) (U. Sulaeman).

<https://doi.org/10.1016/j.surfin.2021.101672>

Received 19 October 2021; Received in revised form 26 November 2021; Accepted 7 December 2021

Available online 17 December 2021

2468-0230/© 2021 Elsevier B.V. All rights reserved.

photogenerated electron can easily transfer to MWCNTs, leading to high charge separation. The surface modification using a conjugated polyvinyl alcohol derivative (CDPVA) can be applied in  $\text{Ag}_3\text{PO}_4$  using chemisorption and heat treatment [8]. This method has significantly suppressed the aggregation of particles, increased the visible-light absorbance, and resulted in more efficient separation of the electron-hole pairs. The core-shell structure of  $\text{Ag}_3\text{PO}_4$  can be designed using a polymer of polyaniline (PANI) [9]. This modification can generate a  $\pi$ -conjugated structure of PANI and the hybridization effect on the surface of  $\text{Ag}_3\text{PO}_4$  that could improve stability and activity. The energy level of PANI also matched with  $\text{Ag}_3\text{PO}_4$  which leads to high separation of electron-hole pairs thus enhancing the photocatalytic ability. PANI shell can also inhibit the  $\text{Ag}_3\text{PO}_4$  dissolution during the photocatalytic reaction. The polyethylene glycol (PEG) also can be used for surface modification of  $\text{Ag}/\text{Ag}_2\text{O}/\text{Ag}_3\text{PO}_4/\text{Bi}_2\text{WO}_6$  composite [10]. This modification leads to small particle size, high specific surface area, and strong visible light absorption. Polydopamine (PDA) can also effectively be used to modify the surface of reduced graphene (RGO) oxide and  $\text{Ag}_3\text{PO}_4$  to form a PDA/RGO/ $\text{Ag}_3\text{PO}_4$  membrane [11]. This engineered membrane enhanced the hydrophilicity properties of the surface. The hydrophilicity was induced by PDA due to a lot of oxygen-containing groups. Because of these excellent findings above, the application of the polymer in  $\text{Ag}_3\text{PO}_4$  surface modification is very promising. Another approach, a natural polymer application to improve the properties of  $\text{Ag}_3\text{PO}_4$ , should also be expected.

The most interesting natural polymer for photocatalyst surface modification is alginate. Alginate is one of the natural compounds that can be applied to improve the properties of photocatalysts, such as  $\text{TiO}_2$  [12],  $\text{ZnO}$  [13], and  $\text{CdS}$  [14]. Alginate generally is derived from brown seaweed which has a structure of a linear copolymer containing a block (1,4)-linked-D-mannuronate (M) and L-guluronate (G) residues [15]. A floating material can be designed using alginate through  $\text{TiO}_2/\text{CaAlg}$  composites using the ionotropic gelation method [12]. This material can be utilized for the removal of tartrazine dye under UV-A irradiation. The floating of photocatalyst is very useful due to easy separation from a treated liquid. A core-shell structure of photocatalyst can also be designed using alginate [16]. In these cases, the floating ability can be enhanced through an internal cavity built by ice-templating. This modification improved the photocatalytic efficiency that was environmentally friendly and conveniently reclaimable. The strong interaction of alginate aerogel and  $\text{TiO}_2$  nanoparticles through Ti-O-C was identified using XPS [17]. This interaction leads to improved electron transfer and increased photogenerated charge separation.

Up to now, there are not so many reports of alginate application in  $\text{Ag}_3\text{PO}_4$ . Some reports are the design of  $\text{CaAlg}/\text{nano-Ag}_3\text{PO}_4$  photocatalyst via in-situ synthesis [18] and  $\text{Ag}_3\text{PO}_4$ -alginate beads [19]. The  $\text{CaAlg}/\text{nano-Ag}_3\text{PO}_4$  are designed via in-situ synthesis resulting in a photocatalyst that has less flammable gas leading to application for fire protection. The  $\text{Ag}_3\text{PO}_4$ -alginate beads can be synthesized by a simple precipitation method [19]. This material exhibited high performance for the degradation of MB and can maintain the activity to five cycles.

In this work, the surface modification using sodium alginate was demonstrated to achieve a highly active  $\text{Ag}_3\text{PO}_4$  photocatalyst. The  $\text{Ag}_3\text{PO}_4$  was synthesized by the precipitation method using  $\text{CaHPO}_4/\text{hydroxyapatite}$  composite as source phosphate ion and silver nitrate in the ethanol solution. The single phase of  $\text{Ag}_3\text{PO}_4$  was precipitated. Incorporating alginate on the surface of this phase significantly improved photocatalytic activity. The alginate was successful chemically bonded on the surface of  $\text{Ag}_3\text{PO}_4$ .

## 2. Experimental

### 2.1. Synthesis of photocatalyst

The chemicals of  $\text{AgNO}_3$  (Reag. Ph Eur, Merck),  $\text{KH}_2\text{PO}_4$  (analytical grade, Merck),  $\text{CaCl}_2$  (Reag. Ph Eur, Merck),  $\text{NaOH}$  (analytical grade,

Merck), and sodium alginate (Sigma-Aldrich) were used for the preparation of samples.

The photocatalyst samples were prepared using  $\text{AgNO}_3$  and the  $\text{CaHPO}_4/\text{hydroxyapatite}$  composite as a source of phosphate. To prepare the composite, the 100 mL of 1 M  $\text{CaCl}_2$  solution was added dropwise to the 100 mL of 0.6 M  $\text{KH}_2\text{PO}_4$  solution until white suspension formed. The ratio of both solutions was adjusted at 8 using a 0.1 M  $\text{NaOH}$  solution. The suspension was aging for 12 h, then the white precipitate was separated by filtration, washed three-time and dried in an oven for 12 h at  $60^\circ\text{C}$  [20].

To synthesize the photocatalyst samples, firstly the ethanol solution was prepared by mixing ethanol and water at the ratio of 1:1 [21]. The  $\text{AgNO}_3$  ethanol solution was prepared by dissolving 0.85 g of  $\text{AgNO}_3$  into 100 mL of ethanol solution. The white  $\text{CaHPO}_4/\text{hydroxyapatite}$  powder of 0.40 g was suspended into 25 mL of water. This suspension was reacted slowly (dropwise) to an  $\text{AgNO}_3$  ethanol solution until the white suspension disappeared and changed into a yellow suspension. This yellow precipitate was separated by filtration, washed with acetone and water, dried in an oven for 12 h at  $60^\circ\text{C}$ . This prepared sample was named AP-H. The sample of  $\text{Ag}_3\text{PO}_4$  which was not using  $\text{CaHPO}_4/\text{hydroxyapatite}$  composite as phosphate source also prepared for photocatalytic comparison. This sample was prepared using  $\text{KH}_2\text{PO}_4$  solution directly as a source of phosphate and the sample was named AP.

The incorporating alginate on AP-H was prepared using the chemisorption method. A certain amount of sodium alginate was dissolved into 50 mL of water. The 0.6 g AP-H were added to the alginate solution, stirred for 12 h at room temperature. The precipitate was separated using centrifugation at 1500 rpm, washed with acetone and water 3 times in beaker glass, and dried in an oven at  $60^\circ\text{C}$  for 4 h. The variation alginate solution was designed using 0.3 g, 0.6 g, 0.9 g, 1.2 g, 1.5 g, 1.8 g, and 2.1 g of sodium alginate which are named AP-HG03, AP-HG06, AP-HG09, AP-HG12, AP-HG15, AP-HG18, and AP-HG21, respectively.

### 2.2. Characterization of photocatalysts

The structures of AP, AP-H, and AP-HG15 samples were characterized using XRD (PANalytical Aeris). The XRD analysis was carried out using Cu-K $\alpha$  incident source at the range of  $2\theta$  from  $5^\circ$  to  $80^\circ$  with the step size of  $0.017^\circ$ . The  $K\alpha_1$ ,  $K\alpha_2$ , and  $K\beta$  of the light source are 1.54060 Å, 1.54443 Å, 1.39225 Å, respectively, with the  $K\alpha_2/K\alpha_1$  ratio of 0.5. The diffraction patterns were refined by the Rietveld method using the HighScore Plus software. Absorption spectra of these samples and sodium alginate were investigated using UV-Vis DRS (Shimadzu UV-2450). To evaluate the separation of photogenerated electrons and holes, the photoluminescence (PL) spectra were carried out using a laser diode at 405 nm, 60 milliWatts as an excitation source. The emission was recorded by a portable MAYAPRO2000 spectrometer from Ocean Optics. The surface functional groups of samples were studied using FTIR (Shimadzu IR Prestige 21). Specific surface area, pore-volume, and pore size of these samples were also measured using the BET (Micromeritics TriStar II 3020). SEM (JEOL JSM-7800F) was utilized to investigate the morphology of AP-H and AP-HG15 samples. The AP-HG15 morphology was also investigated using TEM (ThermoFisher Talos F200X). To understand the interaction of alginate on the surface of photocatalyst, the sample of AP-H and AP-HG15 were analyzed using XPS (ULVAC PHI 5600) and the deconvolution was carried out using XPS software (XPSPEAK Version 4.1).

### 2.3. Photocatalysis and mechanism evaluation

The Rhodamine B (RhB) solution with the concentration of 10 mg/L was utilized as a model of wastewater for photodegradation [22]. The photocatalyst of 0.2 g was added to 250 mL of RhB solutions, stirred under a magnetic stirrer at a speed of 400 rpm. The photocatalytic evaluation was evaluated under dark and irradiated conditions for 20 min and 50 min, respectively. Blue LED was used as a source of



irradiation [4]. Samples of 4 ml were taken out from the solution every 10 min, centrifuged at 5000 rpm. The RhB concentration was measured using a spectrophotometer. To ensure the effect of alginate on the surface of photocatalyst, the photocatalytic activity was also applied to methylene blue (MB) and methyl orange (MO) photodegradation. The cyclic photocatalytic activity of AP-H and AP-HG15 were investigated for 5 cycles. The mechanism of reaction in the surface was evaluated using isopropyl alcohol (IPA), benzoquinone (BQ), and ammonium oxalate (AO) for detecting the effect of  $\bullet\text{OH}$ ,  $\bullet\text{O}_2^-$  and  $\text{h}^+$ , respectively [23]. The red light irradiation of LED was also applied to AP-H and AP-HG15 to analyze the effect of alginate.

### 3. Results and discussion

#### 3.1. Characterization of photocatalyst

The diffraction peaks of three samples were fully indexed to the cubic structure of  $\text{Ag}_3\text{PO}_4$ , matched with the data of ICSD 98-020-1362 with the space group of  $\text{P-43n}$  (218) (Fig. 1). No other phase was observed in the XRD pattern, confirming that the structures are single phases. It is well known that a structural unit of  $\text{Ag}_3\text{PO}_4$  is a body-centered-cubic lattice with a regular  $\text{PO}_4$  tetrahedron [24]. The P atom is coordinated with four oxygen atoms forming the  $\text{PO}_4$  tetrahedra and the Ag atom is surrounded by four oxygen atoms forming the  $\text{AgO}_4$  tetrahedra, whereas the O atom is coordinated with three Ag atoms and one P atom. Three  $\text{AgO}_4$  tetrahedra and one  $\text{PO}_4$  tetrahedron are connected by the corner oxygen [25].

The different characteristic of the XRD profile was found in the (210) peak, shown in the insert of Fig. 1. Rietveld refinement analysis was carried to investigate the peaks (Fig. S1 in the Supplementary Material). The doublet peak of (210) was observed in the XRD profile for  $\text{Ag}_3\text{PO}_4$  prepared using  $\text{KH}_2\text{PO}_4$  and  $\text{AgNO}_3$  (AP). It might be caused by the energy source of XRD that contains two lines ( $\text{K-}\alpha_1$  and  $\text{K-}\alpha_2$ ) with an intensity ratio of 2:1 [26]. The AP sample exhibited the angle ( $2\theta$ ) of  $33.1909^\circ$  and  $33.2758^\circ$  with the intensity of 4687 counts and 2343 counts for the source of  $\text{K-}\alpha_1$  and  $\text{K-}\alpha_2$ , respectively. When using the composite precursor ( $\text{CaHPO}_4/\text{hydroxyapatite}$ ), this doublet peak disappeared as shown in AP-H sample. It indicates that the preparation using the precursor of composite might cause a broadening of peak x-ray diffraction. The full width at half maximum (FWHM) of  $0.0871^\circ$ ,  $0.107^\circ$ , and  $0.139^\circ$  was estimated for the sample of AP, AP-H, and AP-HG15, respectively (Table S1 in the Supplementary Material). The increased FWHM due to peak broadening in AP-H sample might be caused by the defect formation [27]. The defects can be created from the structural arrangement, synthetic method, and experimental conditions [28]. The alginate treatment on the surface of  $\text{Ag}_3\text{PO}_4$  also significantly leads to a broad peak XRD shown in AP-HG15. The alginate treatment on the

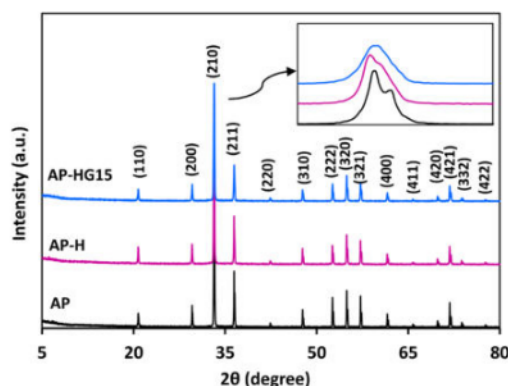


Fig. 1. XRD patterns of AP, AP-H, and AP-HG15.

sample can influence the particle size through the eroded particle on the surface. This phenomenon can lead to a broad peak of XRD. It is also well known that the peak broadening occurred in the crystal due to a crystallite smallness, micro-stresses, and chemical heterogeneities [27]. This prominent characteristic confirms that the alginate might influence the properties of  $\text{Ag}_3\text{PO}_4$ .

The source of starting material significantly affected  $\text{Ag}_3\text{PO}_4$  synthesis. This preparation applied the  $\text{CaHPO}_4/\text{hydroxyapatite}$  as a source of phosphate ion. This starting material was obtained through the reaction of  $\text{KH}_2\text{PO}_4$  and  $\text{CaCl}_2$  under pH 8, resulting in white suspension of  $\text{CaHPO}_4/\text{hydroxyapatite}$  composite. The XRD pattern of this composite and the reaction step formation can be seen in Fig. S2 in the Supplementary Material. It was successful that AP-H synthesized through this step resulting in a single phase of the structure. There is no  $\text{CaHPO}_4$  or hydroxyapatite was found in the XRD pattern of AP-H, indicating the phosphate ion released from this material and creating a phase of  $\text{Ag}_3\text{PO}_4$ . This phase could lead to a different property such as absorption and photoluminescence (PL) spectra compared to AP prepared directly with  $\text{KH}_2\text{PO}_4$  and  $\text{AgNO}_3$ . To make sure there is no  $\text{CaHPO}_4/\text{hydroxyapatite}$ , the Ca atom on the surface of  $\text{Ag}_3\text{PO}_4$  was analyzed using high resolution of XPS (Fig. S3 in the Supplementary Material). The atomic percentage of 0.24% and 0.11% were found in the sample of AP-H and AP-HG15, respectively. After  $\text{Ar}^+$  sputtering, the Ca content decreased to 0.14% and 0.00% for the sample of AP-H and AP-HG15, respectively. All the Ca atomic percentages are very small suggesting that the Ca-based compounds do not significantly exist.

The DRS absorptions of AP, AP-H, and AP-HG15 are displayed in Fig. 2. AP-H and AP-HG15 gave a higher absorption in the visible region above  $\sim 223\text{nm}$ . This phenomenon might be related to the source of phosphate from  $\text{CaHPO}_4/\text{hydroxyapatite}$  that might induce defect formation. This result was similar to the previous report that the strong absorption in the visible region was created after using the hydroxyapatite as a phosphate source in the preparation of  $\text{Ag}_3\text{PO}_4$  [20]. It is very beneficial since the visible light responsive photocatalyst is needed to implement in sunlight irradiation, more absorption in visible light more electrons can be excited. The spectra absorptions were detail analyzed using Tauc's relation [29]. The edge absorptions at 512 nm, 521 nm, and 521 nm were found in the sample of AP, AP-H, and AP-HG15, respectively, suggesting that all samples can be well activated under blue light irradiation. The bandgap energies of 2.42 eV, 2.38 eV, and 2.38 eV were estimated for AP, AP-H, and AP-HG15, respectively (Fig. S4 in the Supplementary Material). The lower bandgap energy of AP-H and AP-HG15 might be created by different phosphate sources. The

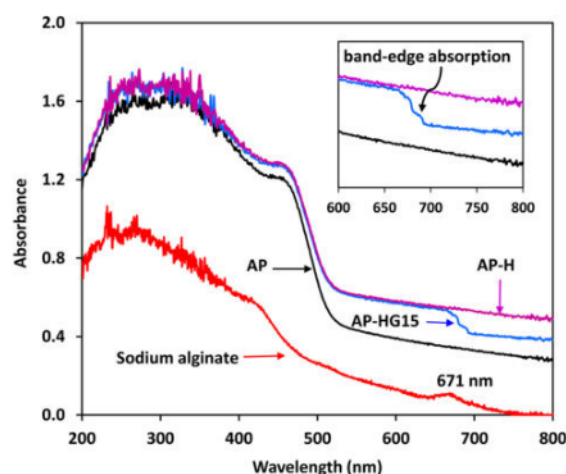


Fig. 2. Absorption spectra of AP, AP-H, AP-HG15, and sodium alginate.

incorporation of alginate on the surface of  $\text{Ag}_3\text{PO}_4$  created a new band-edge absorption at 729 nm that can be converted to 1.70 eV of bandgap energy (insert Fig. 2). This new phenomenon in absorption might be generated by the interaction of alginate and AP-H forming a new conjugate. The sodium alginate, a material applied for the modification, was also had a small absorption at 671 nm. It might induce the new edge absorption formation of  $\text{Ag}_3\text{PO}_4$ .

The PL spectra are very useful to assess the photogenerated charge separation of photocatalysts [30]. Fig. 3 displayed the PL spectra of AP, AP-H and AP-HG15 under the excitation wavelength of 405 nm. The PL spectra of AP exhibited high three strong emission peaks at 533, 561 and 599 nm, which were related to the recombination of photogenerated electron and hole pairs of  $\text{Ag}_3\text{PO}_4$ . The decreased emission of AP-H, mainly in a lower wavelength of 599 nm, implies that the synthesis of  $\text{Ag}_3\text{PO}_4$  using the composite of  $\text{CaHPO}_4$ /hydroxyapatite as a source of phosphate ion prevents the recombination rate. It might be the defect formation in  $\text{Ag}_3\text{PO}_4$  effectively trapping the photogenerated electron. The lowest PL spectra at 533 and 561 nm peak emissions were found in AP-HG15 indicating that the alginate effectively improves the separation of photogenerated electrons and holes.

The absorption spectra of AP, AP-H, and AP-HG15 were also investigated using FTIR ranging from 400 to 4000  $\text{cm}^{-1}$ . All samples are similar absorption (except for the AP-HG15) as shown in Fig. 4. A broad absorption at around 3130  $\text{cm}^{-1}$  is attributed to O–H stretching vibration, whereas the peak of 1675  $\text{cm}^{-1}$  is attributed to H–O–H bending vibration from the water adsorbed on the surface of  $\text{Ag}_3\text{PO}_4$  [31]. The absorption of 1080  $\text{cm}^{-1}$  was assigned to C–O stretching [32] that might have originated from the carbon-based compound impurities. The peak of 859  $\text{cm}^{-1}$  and 989  $\text{cm}^{-1}$  may refer to symmetrical stretching and asymmetric stretching vibrations of P–O–P groups, respectively [33]. The strong absorption at 543  $\text{cm}^{-1}$  was assigned to the bending vibration of O=P–O [34]. Specific vibration among the samples was found at 1032  $\text{cm}^{-1}$  assigned to saccharide structure (C–O–C stretching) of AP-HG15 [35].

The BET surface area, pore-volume, and pore diameter of AP, AP-H and AP-HG15 were measured, and the results can be seen in Table 1. There are no significant changes in specific surface area, pore-volume, and pore diameter implying that the enhanced photocatalytic activity might not be influenced by these characteristics.

The SEM images of AP-H and AP-HG15 can be seen in Fig. 5a and b. Sphere and irregular shape with the distribution of 200–1000 nm was observed in both AP-H and AP-HG15. Carbon-based compound impurities attached to the surface were found in both AP-H and AP-HG15. The average particle sizes of 618 and 492 nm can be calculated using ImageJ processing for AP-H and AP-HG15 samples, respectively (Fig. 5c and d). The smaller particle of AP-HG15 might be induced by alginate. Small

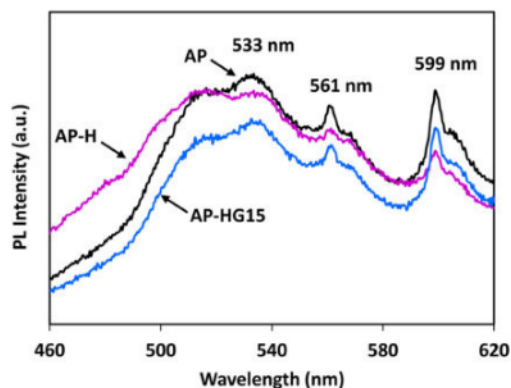


Fig. 3. PL spectra of AP, AP-H, and AP-HG15 at the excitation wavelength of 405 nm.

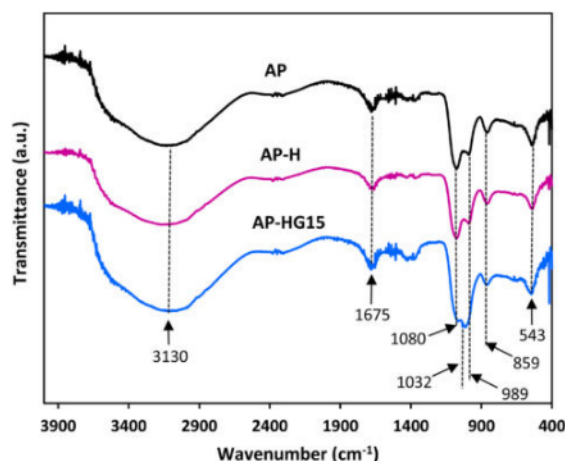


Fig. 4. FTIR spectra of AP, AP-H, and AP-HG15.

Table 1  
BET surface area, pore volume, and pore diameter of AP, AP-H and AP-HG15.

Samples	BET surface area ( $\text{m}^2/\text{g}$ )	Pore volume ( $\text{cm}^3/\text{g}$ )	Pore diameter (nm)
AP	0.776	0.0036	18.73
AP-H	0.673	0.0022	13.17
AP-HG15	0.901	0.0035	15.41

fragments can be originated from the eroded large agglomerates. Fig. 5e and f showed the several sphere particles of AP-HG15 which alginate might be chemically bonded on the surface.

### 3.2. XPS analysis

The effect of alginate on the surface of  $\text{Ag}_3\text{PO}_4$  was studied using XPS. The core level of Ag 3d, P 2p, and O 1s was compared between the sample of AP-H and AP-HG15. These spectra were shown in Fig. 6. There are significant changes in binding energies (BEs) and FWHM (full-width at half-maximum) after alginate treatment. The BEs of 374.3 eV and 368.3 eV were found at peaks of  $\text{Ag}3d_{3/2}$  and  $\text{Ag}3d_{5/2}$ , respectively for AP-H [36], these BEs decreased to 374.0 and 368.0 as found in AP-HG15. There is a shift of 0.3 eV after incorporating with alginate. The FWHM of 1.44 and 1.47 were measured at  $\text{Ag}3d_{3/2}$  and  $\text{Ag}3d_{5/2}$ , respectively for AP-H, whereas the larger FWHM of 1.49 and 1.59 was found in AP-HG15, respectively.

To obtain detailed information, the deconvolution of P 2p and O 1s spectra were studied, the results can be seen in Fig. 7. The BEs of 134.3 eV and 133.1 eV were assigned to  $\text{P}2p_{1/2}$  and  $\text{P}2p_{3/2}$ , respectively, found in AP-H [37]. These BEs shifted to 133.8 eV and 132.6 eV, respectively after being treated with alginate as shown in the sample of AP-HG15. There is a shift of 0.5 eV after alginate treatment. The FWHM of 1.64 eV and 1.71 eV was calculated to  $\text{P}2p_{1/2}$  and  $\text{P}2p_{3/2}$  of AP-H, respectively, whereas the lower FWHM of 1.59 eV and 1.54 eV was found in AP-HG15 for  $\text{P}2p_{1/2}$  and  $\text{P}2p_{3/2}$ , respectively. From this data, the alginate treatment narrowed the P 2p spectra but broadened the Ag 3d spectra implying that alginate might be strongly attracted to these elements. The deconvolution of O 1s was displayed in Fig. 7c and d. The BEs of 530.9 and 532.7 eV in AP-H sample were assigned to oxygen lattice (I) and oxygen hydroxyl/organic compound (II), respectively [38]. These BEs shifted to 530.6 eV and 532.5 eV after being treated with alginate as found in the AP-HG15 sample. There is a BE shift of 0.3 eV and 0.2 eV for oxygen I and II respectively. The peak of oxygen II in AP-HG15 is higher

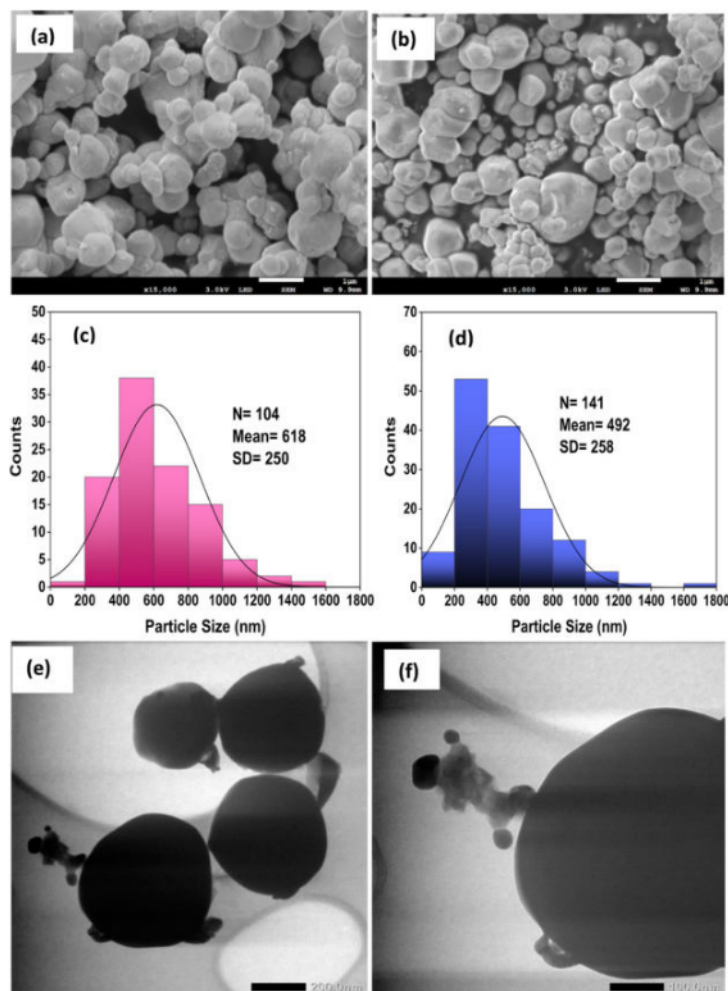


Fig. 5. SEM images of AP-H (a), AP-HG15 (b), the particle size distribution of AP-H (c), AP-HG15 (d), and TEM images of AP-HG15 (e) with higher magnification (f).

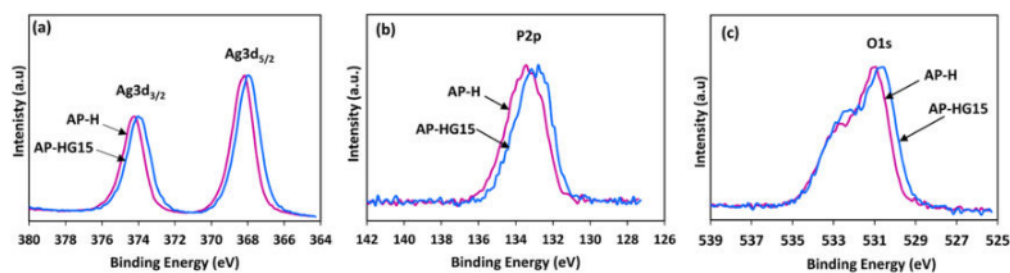


Fig. 6. XPS of Ag3d (a), P2p (b), and O1s (c) for the samples of AP-H and AP-HG15.

due to the oxygen contribution of alginate on the surface of  $\text{Ag}_3\text{PO}_4$ .

The spectra of C1s and their deconvolution can be seen in Fig. 8. The carbon-based compound impurities were found in both AP-H and AP-HG15. The C1s spectra of AP-HG15 were larger and broader, indicating that the alginate was successfully incorporated on the surface (Fig. 8a). The alginate has remained attached on the surface after treatment with the  $\text{Ar}^+$  sputtering as found in the sample of AP-HG15

(Fig. 8b), suggesting that alginate was strongly bonded on the surface of photocatalyst. Whereas, the carbon-based compound impurities in AP-H were completely disappeared after  $\text{Ar}^+$  sputtering. The deconvolution of C1s AP-HG15 was displayed in Fig. 8c. The BEs of 284.6 eV, 286.2 eV, 287.3 eV, and 288.7 eV were assigned to C-C/C-H, C-O/C-O-C, C=O, and O-C=O, respectively [39]. These peaks still existed after  $\text{Ar}^+$  sputtering, as shown in Fig. 8d.



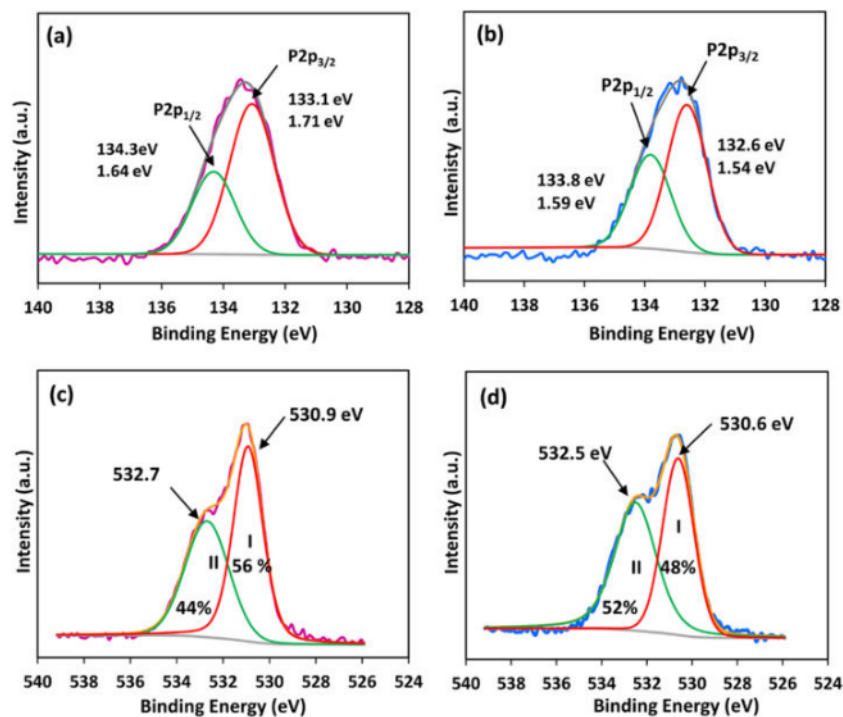


Fig. 7. XPS deconvolution of P2p AP-H (a), P2p AP-HG15 (b), O1s AP-H (c), and O1s AP-HG15 (d).

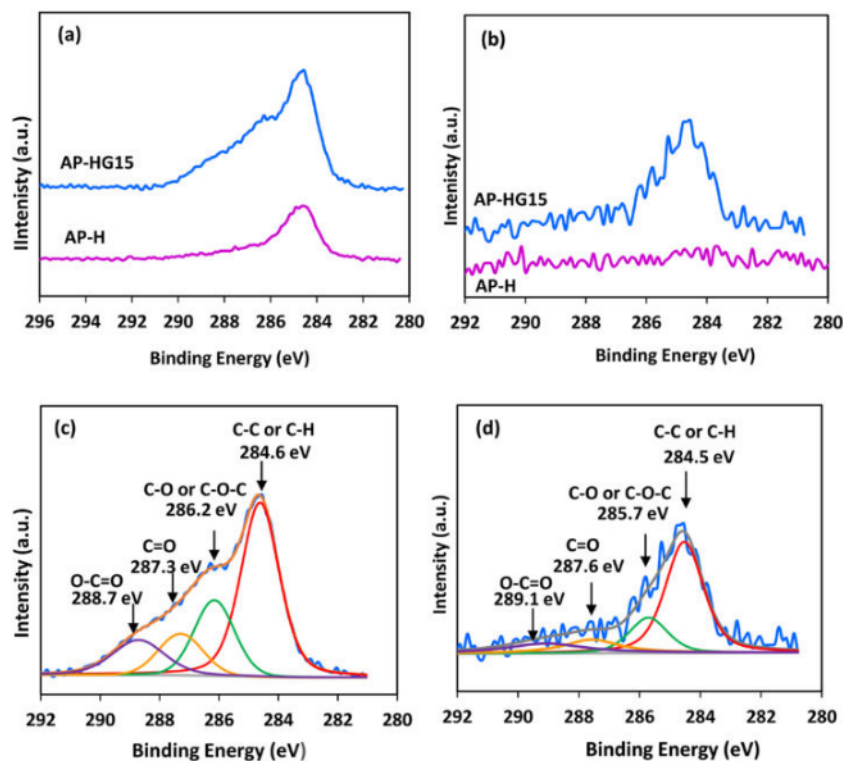


Fig. 8. C1s XPS of AP-H and AP-HG15 (a), C1s after Ar<sup>+</sup> sputtering treatment (b), and C1s deconvolution of AP-HG15 (c) and after Ar<sup>+</sup> sputtering treatment (d).

The Ag/P atomic ratios of 2.98 and 2.43 were found in AP-H and AP-HG15, respectively (before Ar<sup>+</sup> sputtering). The lower atomic ratio of Ag/P in AP-HG15 might be caused by attaching alginate to the surface of Ag<sub>3</sub>PO<sub>4</sub>. A small portion of silver ion on the surface might be replaced by the functional group of alginates leading to a lower Ag<sup>+</sup> content in the surface. The interaction of the alginate carboxyl group with a phosphate ion, forming the covalent bond of P–O–C. The interaction of alginate carboxyl with Ag<sup>+</sup> ion might also be possible forming the ionic interaction of Ag–O–C. The chemical interaction can be illustrated in Fig. 9. These interactions lead to higher electron delocalization of alginate on the surface of Ag<sub>3</sub>PO<sub>4</sub> that generates the small edge absorption at 729 nm as shown in Fig. 2. This chemical bonding can help improve the transport of charge carriers that lead to the high efficiency of the photocatalytic reaction.

The Ag/P atomic ratio of 2.86 and 3.06 was found in AP-H and AP-HG15, after Ar<sup>+</sup> sputtering, respectively. The higher atomic ratio of Ag/P in AP-HG15 might be caused by the loss of phosphate ions on the surface. Since the strong covalent interaction between phosphate and carboxyl group, the phosphate ion might be swept out together with portion alginate after Ar<sup>+</sup> sputtering, leading to the lower content of phosphor in the surface of AP-HG15, therefore the atomic ratio of Ag/P increased.

### 3.3. Photocatalytic evaluation

The evaluation of photocatalytic activity was conducted on the samples with alginate content variation from 0.3 g to 2.1 g. The pseudo-first-order-kinetic of  $\ln(C_0/C) = kt$  were applied to identify the characteristic of photocatalytic reactions [21]. C and C<sub>0</sub> are the RhB concentration at time t and zero respectively, k is the pseudo-first-order rate constant (min<sup>−1</sup>). The results can be displayed in Fig. 10.

The average rate constants of 0.0198 min<sup>−1</sup>, 0.0298 min<sup>−1</sup>, 0.0545 min<sup>−1</sup>, 0.0708 min<sup>−1</sup>, 0.0786 min<sup>−1</sup>, 0.0840 min<sup>−1</sup>, 0.0909 min<sup>−1</sup>, 0.0563 min<sup>−1</sup> and 0.0307 min<sup>−1</sup> were calculated from the sample of AP, AP-H, AP-HG03, AP-HG06, AP-HG09, AP-HG12, AP-HG15, AP-HG18, and AP-HG21, respectively. With the increase of alginate concentration, the photocatalytic activity increased and the highest activity was found at 1.5 g of alginate (AP-HG15). After more addition of alginate, the photocatalytic activity decreased. The higher alginate content on the surface of the photocatalyst might hinder the light penetration lead to decreased activity. The highest activity of AP-HG15 was found 4.6 times higher compared to the Ag<sub>3</sub>PO<sub>4</sub> and 3.0 times higher compared to AP-H.

To ensure the high photocatalytic ability of AP-HG15, the comparison of AP-H and AP-HG15 was also applied to MB and MO degradation. The result can be seen in Fig. 11. For MB degradation, the rate constant of 0.010 min<sup>−1</sup> was measured in a sample of AP-H and significantly increased to 0.041 min<sup>−1</sup> in AP-HG15 when alginate was treated on the surface. It was 4.1 higher compared to AP-H. For MO degradation, the rate constant of 0.0057 was found in AP-H and enhanced to 0.011 in AP-HG15. It was 1.9 times higher compared to AP-H. Based on the photocatalytic tests, the alginate surface modification improves photocatalytic activity.

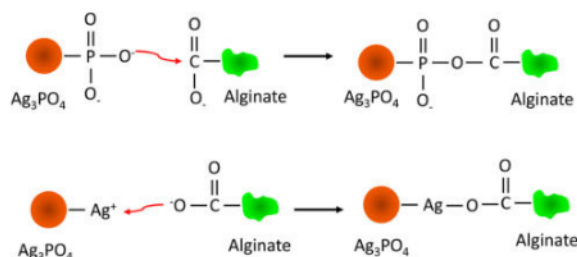


Fig. 9. The interaction of alginate on the surface of Ag<sub>3</sub>PO<sub>4</sub>.

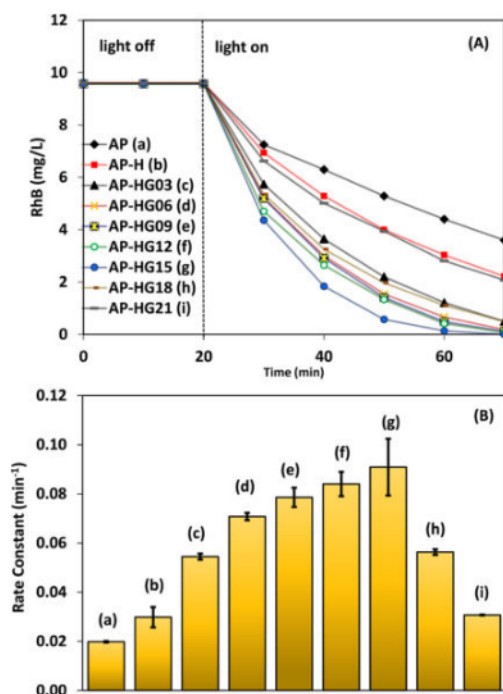


Fig. 10. The RhB photodegradation using Ag<sub>3</sub>PO<sub>4</sub> photocatalyst with the variation of alginate content (0.3–2.1 gram (A), and the average rate constants of pseudo-first-order kinetic (B).

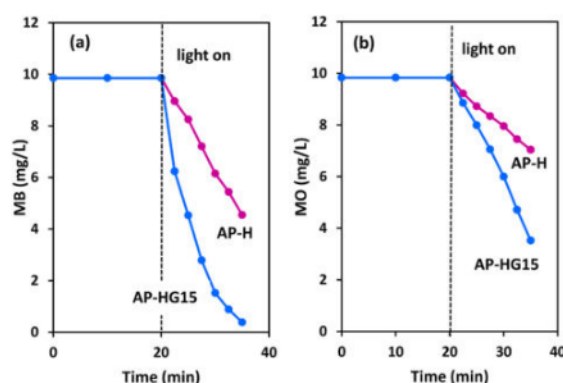


Fig. 11. The photodegradation of methylene blue (MB) (a), and methyl orange (MO) (b) using photocatalysts of AP-H and AP-HG15.

The cycle of photocatalytic activity of AP-H and AP-HG15 was also compared [Fig. 12]. The rate constant of 0.0269 min<sup>−1</sup>, 0.0163 min<sup>−1</sup>, 0.0078 min<sup>−1</sup>, 0.0061 min<sup>−1</sup>, 0.0032 min<sup>−1</sup> was measured for cycle 1, cycle 2, cycle 3, cycle 4, and cycle 5 of AP-H sample, respectively. Whereas the rate constant of 0.0827 min<sup>−1</sup>, 0.0449 min<sup>−1</sup>, 0.0310 min<sup>−1</sup>, 0.0174 min<sup>−1</sup> and 0.0125 min<sup>−1</sup> was obtained from cycle 1, cycle 2, cycle 3, cycle 4, and cycle 5 of AP-HG15, respectively. Every cycle of the AP-HG15 showed higher activity compared to the AP-H, indicating that the alginate-modified surface exhibited a significant effect. The gradual decrease due to the cycling test might be caused by metallic Ag formation from photo-corrosion [20,40]. The samples of AP-H and AP-HG15 after cyclic test of photocatalytic reaction were investigated



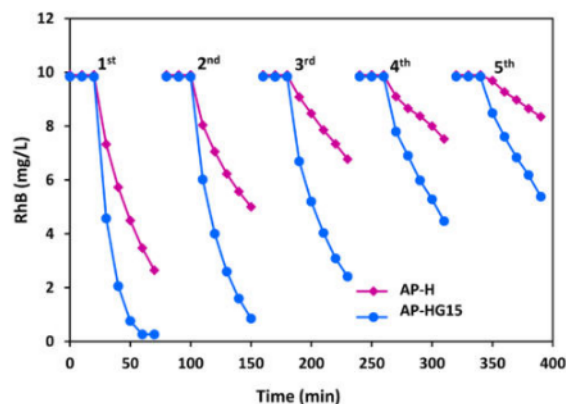


Fig. 12. The cyclic photocatalytic activity of AP-H ( $\text{Ag}_3\text{PO}_4$  prepared without alginate) and AP-HG15 ( $\text{Ag}_3\text{PO}_4$  prepared with alginate).

using XRD. Both AP-H and AP-HG15 exhibited a metallic Ag ( $\text{Ag}^0$ ), indicating that the photoreduction occurred on the surface. The content of  $\text{Ag}^0$  in AP-HG15 is lower than that of AP-H, suggesting that the alginate can suppress the photoreduction of  $\text{Ag}^+$  as shown in Fig. S5 in the Supplementary Material.

#### 3.4. Mechanism of photocatalytic reaction

The mechanism of photocatalytic activity was investigated using ammonium oxalate (AO), isopropyl alcohol (IPA), and benzoquinone (BQ) as a scavenger of holes ( $\text{h}^+$ ), hydroxyl radical ( $\bullet\text{OH}$ ), and superoxide radicals ( $\text{O}_2^{\bullet-}$ ), respectively [23]. After the addition of scavenger, all rate constant of photocatalytic activity decreased (Fig. 13a and b). The rate constants of  $0.0326 \text{ min}^{-1}$ ,  $0.0213 \text{ min}^{-1}$ ,  $0.0135 \text{ min}^{-1}$ , and  $0.0060 \text{ min}^{-1}$  were calculated in AP-H for blank, IPA, BQ, and AO, respectively. Whereas the rate constant of  $0.0957 \text{ min}^{-1}$ ,  $0.0560 \text{ min}^{-1}$ ,

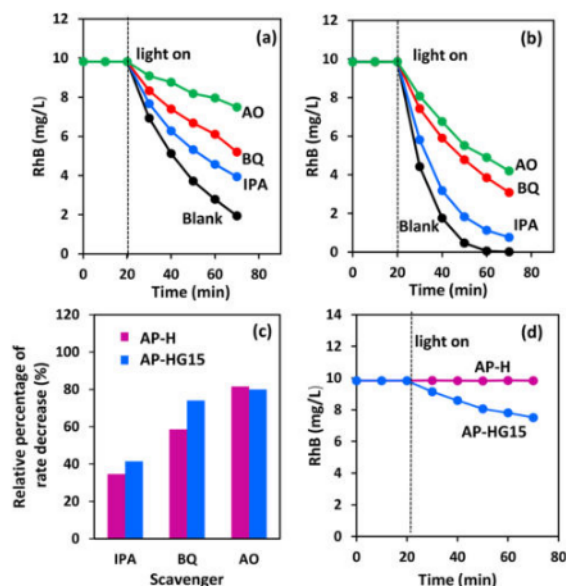


Fig. 13. The photocatalytic activity of AP-H (a), AP-HG15(b), with the variation of scavenger (IPA, BQ, AO), the relative percentage of rate decrease (c), and the effect of red light (627 nm) irradiation on the samples (d).

$0.0248 \text{ min}^{-1}$ , and  $0.192 \text{ min}^{-1}$  were found in AP-HG15 for blank, IPA, BQ, and AO, respectively. The relative percentages of rate decrease in the sample can be approximated by  $(k_b - k_s)/k_b \times 100\%$ , where  $k_b$  is the rate constant of blank (without scavenger),  $k_s$  is the rate constant of a scavenger. The results of the photocatalytic mechanism are displayed in Fig. 13c. The relative percentages of rate decrease in AP-H were 36%, 61%, 82% for IPA, BQ, and AO, respectively, whereas in AP-HG15 sample were 41%, 74%, 80% for IPA, BQ, and AO, respectively. Both AP-H and AP-HG15 have the same order of radical role on the surface of the photocatalytic reaction,  $\text{h}^+ > \text{O}_2^{\bullet-} > \bullet\text{OH}$ . They have the same high  $\text{h}^+$  role in the photocatalytic reaction. Alginate surface modification (AP-HG15) enhances the role of  $\text{O}_2^{\bullet-}$  and  $\bullet\text{OH}$ . The increased role of  $\text{O}_2^{\bullet-}$  may be due to the alginate chemical bonding on the surface of AP-HG15 which forms a new conjugate. This is supported by the absorbance feature which has a band-edge absorption at 729 nm (1.70 eV). This conjugate can act as an electron donor and promote the reduction of  $\text{O}_2$  to  $\text{O}_2^{\bullet-}$ . Another radical species that increase in AP-HG15 is  $\bullet\text{OH}$ . The increase in  $\bullet\text{OH}$  may be related to the higher phosphate ion on the surface of AP-HG15 because the ratio of Ag/P atoms in AP-HG15 is lower than that of AP-H which indicates that AP-HG15 has a large phosphate on the surface. The large negative charge of phosphate ions can maintain a large dipole that promotes photogenerated charge separation [41]. The higher negative electrostatic field created  $\text{PO}_3^{4-}$  in the surface can induce holes to flow to the surfaces and increase the formation of  $\bullet\text{OH}$  radicals [1].

The visible light can excite the electron of conjugates and act as an electron donor. To ensure the mechanism, the red light with a longer wavelength of 627 nm was applied on AP-H and AP-HG15 (Fig. 13d). The results showed that there is no activity on AP-H. Surprisingly, the photocatalytic activity for RhB degradation was significantly four times on the AP-HG15, indicating the conjugate molecule on the surface has a significant role in the enhancement of photocatalytic activity.

The proposed mechanism of photocatalytic reaction in the surface of AP-HG15 can be seen in Fig. 14. Upon blue light irradiation, the electron in VB can be excited into CB, producing a hole in VB which oxidizes the hydroxyl ion or water into hydroxyl radical. The conjugate molecule generated on the surface might act as a sensitizer that contributes to producing the photogenerated electron. The electron of HOMO can be excited into the LUMO of the sensitizer that directly transfers to the CB of  $\text{Ag}_3\text{PO}_4$ . The sensitizer can act as an electron donor. This phenomenon enhances the reduction of oxygen to produce more superoxide radicals. Meanwhile, the hole formed in VB of  $\text{Ag}_3\text{PO}_4$  might have migrated to the HOMO of conjugate increasing the separation of photogenerated electrons and holes. The HOMO directly reacts with RhB to produce the degradation products.

#### 4. Conclusions

Alginate can effectively modify the surface of  $\text{Ag}_3\text{PO}_4$  under the chemisorption method. Alginate treatment on the photocatalyst surface broadened the XRD peak and generated a small band-edge absorption at

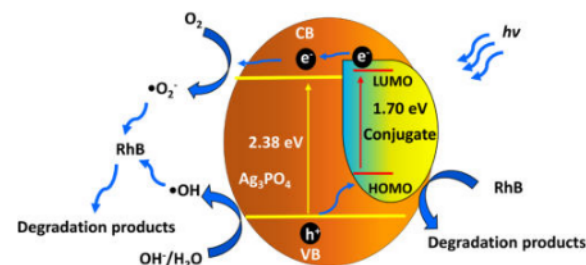


Fig. 14. Mechanism of a photocatalytic reaction on the surface of  $\text{Ag}_3\text{PO}_4$  photocatalyst modified using alginate.

729 nm (1.70 eV). The specific 1032  $\text{cm}^{-1}$  vibration assigned to the C–O–C stretching originates from the alginate on the surface of the photocatalyst. Lower XPS binding energy was observed due to the incorporation of alginate. Shifts of 0.3 eV and 0.5 eV were observed for Ag3d and P2p, respectively. Alginate treatment also increased the FWHM value of Ag3d and decreased the FWHM value of P2p. The different characteristics of XPS indicate that the alginate was successfully chemically bonded to the  $\text{Ag}_3\text{PO}_4$  surface. The interaction of the alginate carboxyl group with phosphate ions can occur in the P–O–C covalent form and interaction with  $\text{Ag}^+$  ions can occur in the Ag–O–C form. The alginate-modified  $\text{Ag}_3\text{PO}_4$  photocatalyst has a higher photocatalytic activity under visible light irradiation. The excellent photocatalytic activity can be induced by the conjugates generated on the surface of the photocatalyst which acts as sensitizers for electron donors. This modification enhances the role of  $\text{O}_2^{\bullet-}$  and  $\bullet\text{OH}$  on the surface of the photocatalytic reaction.

## Supporting information

Supplementary Material

## CRediT authorship contribution statement

**Uyi Sulaeman:** Conceptualization, Methodology, Funding acquisition, Project administration, Writing – original draft, Writing – review & editing. **Yusvirza Khairullah Gandasmita:** Investigation, Formal analysis. **Hartiwi Diastuti:** Data curation, Formal analysis. **Ponco Iswanto:** Software, Validation, Visualization. **Isnaeni Isnaeni:** Formal analysis. **Ardiansyah Taufik:** Formal analysis. **Shu Yin:** Resources, Supervision.

## Declaration of Competing Interest

The authors declare that they have no known competing financial interests or personal relationships that could have appeared to influence the work reported in this paper.

## Acknowledgement

This research was financially supported by the Directorate of Research and Community Service, Ministry of Education, Culture, Research and Technology, the Republic of Indonesia, in the Scheme of World-Class Research (117/SP2H/LT/DRPM/2021).

## Supplementary materials

Supplementary material associated with this article can be found, in the online version, at [doi:10.1016/j.surfin.2021.101672](https://doi.org/10.1016/j.surfin.2021.101672).

## References

- [1] Q. Liu, N. Li, Z. Qiao, W. Li, L. Wang, S. Zhu, Z. Jing, T. Yan, The multiple promotion effects of ammonium phosphate-modified  $\text{Ag}_3\text{PO}_4$  on photocatalytic performance, *Front. Chem.* 7 (2019) 866, <https://doi.org/10.3389/fchem.2019.00866>.
- [2] H. El Masoudi, I. Benabdallah, B. Jaber, M. Benaissa, Enhanced visible light photocatalytic activity of  $\text{Cu}^{2+}$ -doped  $\text{Ag}_3\text{PO}_4$  nanoparticles, *Chem. Phys.* 545 (2021), 111133, <https://doi.org/10.1016/j.chemphys.2021.111133>.
- [3] Y. Ma, J. Li, Y. Jin, K. Gao, H. Cai, G. Ou, The enhancement mechanism of ultra-active  $\text{Ag}_3\text{PO}_4$  modified by tungsten and the effective degradation towards phenolic pollutants, *Chemosphere* 285 (2021), 131440, <https://doi.org/10.1016/j.chemosphere.2021.131440>.
- [4] U. Sulaeman, R.D. Permadi, D.R. Ningsih, H. Diastuti, A. Riapanitra, S. Yin, The surface modification of  $\text{Ag}_3\text{PO}_4$  using anionic platinum complexes for enhanced visible-light photocatalytic activity, *Mater. Lett.* 259 (2020), 126848, <https://doi.org/10.1016/j.matlet.2019.126848>.
- [5] B. Zhang, L. Zhang, Y. Zhang, C. Liu, J. Xia, H. Li, Ionic liquid-assisted synthesis of  $\text{Ag}_3\text{PO}_4$  spheres for boosting photodegradation activity under visible light, *Catalysts* 11 (2021) 788, <https://doi.org/10.3390/catal11070788>.
- [6] X. Li, R. Zheng, Q. Luo, D. Wang, J. An, R. Yin, Y. Liu, D. Wu, X. Han, Cyclized polyacrylonitrile modified  $\text{Ag}_3\text{PO}_4$  photocatalysts with enhanced photocatalytic activity under visible-light irradiation, *Appl. Surf. Sci.* 356 (2015) 941–950, <https://doi.org/10.1016/j.apsusc.2015.08.186>.
- [7] Y. Lin, X. Wu, Y. Han, C. Yang, Y. Ma, C. Du, Q. Teng, H. Liu, Y. Zhong, Spatial separation of photogenerated carriers and enhanced photocatalytic performance on  $\text{Ag}_3\text{PO}_4$  catalysts via coupling with PPy and MWCNTs, *Appl. Catal. B Environ.* 258 (2019), 117969, <https://doi.org/10.1016/j.apcatb.2019.117969>.
- [8] X. Zhu, Y. Shi, Q. Luo, J. An, R. Yin, X. Li, D. Wang, High-efficiency visible-light-driven  $\text{Ag}_3\text{PO}_4$  photocatalysts modified by conjugated polyvinyl alcohol derivatives, *Mater. Res. Express* 6 (2019), 125558, <https://doi.org/10.1088/2053-1591/ab65e5>.
- [9] L. Liu, L. Ding, Y. Liu, W. An, S. Lin, Y. Liang, W. Cui, A stable  $\text{Ag}_3\text{PO}_4$ @PANI core@shell hybrid: enrichment photocatalytic degradation with  $\pi$ - $\pi$  conjugation, *Appl. Catal. B Environ.* 201 (2017) 92–104, <https://doi.org/10.1016/j.apcatb.2016.08.005>.
- [10] Q. Ma, X. Hu, N. Liu, A. Sharma, C. Zhang, N. Kawazoe, G. Chen, Y. Yang, Polyethylene glycol (PEG)-modified  $\text{Ag}/\text{Ag}_2\text{O}/\text{Ag}_3\text{PO}_4/\text{Bi}_2\text{WO}_6$  photocatalyst film with enhanced efficiency and stability under solar light, *J. Colloid Interface Sci.* 569 (2020) 101–113, <https://doi.org/10.1016/j.jcis.2020.02.064>.
- [11] R. Zhang, Y. Cai, X. Zhu, Q. Han, T. Zhang, Y. Liu, Y. Li, A. Wang, A novel photocatalytic membrane decorated with PDA/RGO/ $\text{Ag}_3\text{PO}_4$  for catalytic dye decomposition, *Colloids Surf. A: Physicochem. Eng. Asp.* 563 (2019) 68–76, <https://doi.org/10.1016/j.colsurfa.2018.11.069>.
- [12] I. Dalponte, B.C. de Sousa, A.L. Mathias, R.M.M. Jorge, Formulation and optimization of a novel  $\text{TiO}_2$ /calcium alginate floating photocatalyst, *Int. J. Biol. Macromol.* 137 (2019) 992–1001, <https://doi.org/10.1016/j.ijbiomac.2019.07.020>.
- [13] S.K. Mohamed, Sh.S. Hegazy, N.A. Abdelwahab, A.M. Ramadan, Coupled adsorption-photocatalytic degradation of crystal violet under sunlight using chemically synthesized grafted sodium alginate/ZnO/graphene oxide composite, *Int. J. Biol. Macromol.* 108 (2018) 1185–1198, <https://doi.org/10.1016/j.ijbiomac.2017.11.028>.
- [14] L. Wang, Z. Gao, Y. Li, H. She, J. Huang, B. Yu, Q. Wang, Photosensitization of CdS by acid red-94 modified alginate: dual ameliorative effect upon photocatalytic hydrogen evolution, *Appl. Surf. Sci.* 492 (2019) 598–606, <https://doi.org/10.1016/j.apsusc.2019.06.222>.
- [15] K.Y. Lee, D.J. Mooney, Alginate: properties and biomedical applications, *Prog. Polym. Sci.* 37 (2012) 106–126, <https://doi.org/10.1016/j.progpolymsci.2011.06.003>.
- [16] X.H. Huang, T. Hu, H. Bu, W.X. Li, Z.L. Li, H.J. Hu, W.Z. Chen, M.Z. Lin, Y. Li, G. B. Jiang, Transparent floatable magnetic alginate sphere used as photocatalysts carrier for improving photocatalytic efficiency and recycling convenience, *Carbohydr. Polym.* 254 (2021), 117281, <https://doi.org/10.1016/j.carbpol.2020.117281>.
- [17] J. Dai, Q. Tian, Q. Sun, W. Wei, J. Zhuang, M. Liu, Z. Cao, W. Xie, M. Fan,  $\text{TiO}_2$ -alginate composite aerogels as novel oil/water separation and wastewater remediation filters, *Compos. Part B Eng.* 160 (2019) 480–487, <https://doi.org/10.1016/j.compositesb.2018.12.097>.
- [18] Q. Zhang, X. Zhang, W. Cheng, Z. Li, Q. Li, In situ-synthesis of calcium alginate nano-silver phosphate hybrid material with high flame retardant and antibacterial properties, *Int. J. Biol. Macromol.* 165 (2020) 1615–1625, <https://doi.org/10.1016/j.ijbiomac.2020.10.085>.
- [19] K. Wanchai, Exploitation of  $\text{Ag}_3\text{PO}_4$  impregnated alginate beads for the photocatalytic degradation of dye solution under sunlight irradiation, *Key Eng. Mater.* 751 (2017) 689–694, <https://doi.org/10.4028/www.scientific.net/KEM.751.689>.
- [20] U. Sulaeman, S. Suhendar, H. Diastuti, A. Riapanitra, S. Yin, Design of  $\text{Ag}_3\text{PO}_4$  for highly enhanced photocatalyst using hydroxyapatite as a source of phosphate ion, *Solid State Sci.* 86 (2018) 1–5, <https://doi.org/10.1016/j.solidstatesciences.2018.09.015>.
- [21] U. Sulaeman, D. Hermawan, R. Andreas, A.Z. Abdullah, S. Yin, Native defects in silver orthophosphate and their effects on photocatalytic activity under visible light irradiation, *Appl. Surf. Sci.* 428 (2018) 1029–1035, <https://doi.org/10.1016/j.apsusc.2017.09.188>.
- [22] Y. Liu, C. Liu, C. Shi, W. Sun, X. Lin, W. Shi, Y. Hong, Carbon-based quantum dots (QDs) modified  $\text{ms}/\text{tz-BiVO}_4$  heterojunction with enhanced photocatalytic performance for water purification, *J. Alloy. Compd.* 881 (2021), 160437, <https://doi.org/10.1016/j.jallcom.2021.160437>.
- [23] S. Li, S. Hu, W. Jiang, Y. Liu, J. Liu, Z. Wang, Synthesis of n-type TaON microspheres decorated by p-type  $\text{Ag}_2\text{O}$  with enhanced visible light photocatalytic activity, *Mol. Catal.* 435 (2017) 135–143, <https://doi.org/10.1016/j.mcat.2017.03.027>.
- [24] H.N. Ng, C. Calvo, R. Faggiani, A new investigation of the structure of silver orthophosphate, *Acta Cryst. B* 34 (1978) 898–899, <https://doi.org/10.1107/S0567740878014570>.
- [25] X. Ma, B. Lu, D. Li, R. Shi, C. Pan, Y. Zhu, Origin of photocatalytic activation of silver orthophosphate from first-principles, *Phys. Chem. C* 115 (2011) 4680–4687, <https://doi.org/10.1021/jp111167u>.
- [26] F. Shi, H. Dong, Q. Liu, J. Yang, S. Ren, H. Sun, J. Xiong, Investigation and theoretical calculation of the lattice vibrational spectra of  $\text{BaZrO}_3$  ceramic, *J. Mater. Sci. Mater. Electron.* 28 (2017) 3467–3473, <https://doi.org/10.1007/s10854-016-5944-9>.
- [27] T. Ungár, Microstructural parameters from X-ray diffraction peak broadening, *Scr. Mater.* 51 (2004) 777–781, <https://doi.org/10.1016/j.scriptamat.2004.05.007>.

- [28] G. Botelho, J. Andres, L. Gracia, L.S. Matos, E. Longo, Photoluminescence and photocatalytic properties of  $\text{Ag}_3\text{PO}_4$  microcrystals: an experimental and theoretical investigation, *Chempluschem* 81 (2016) 202–212, <https://doi.org/10.1002/cplu.201500485>.
- [29] M. Mishra, P. Kuppasami, T.N. Sairam, A. Singh, E. Mohandas, Effect of substrate temperature and oxygen partial pressure on microstructure and optical properties of pulsed laser deposited yttrium oxide thin films, *Appl. Surf. Sci.* 257 (2011) 7665–7670, <https://doi.org/10.1016/j.apsusc.2011.03.156>.
- [30] E. Liu, X. Lin, Y. Hong, L. Yang, B. Luo, W. Shi, J. Shi, Rational copolymerization strategy engineered C self-doped  $\text{g-C}_3\text{N}_4$  for efficient and robust solar photocatalytic  $\text{H}_2$  evolution, *Renew. Energy* 178 (2021) 757–765, <https://doi.org/10.1016/j.renene.2021.06.066>.
- [31] S. Yang, D. Zhao, H. Zhang, S. Lu, L. Chen, X. Yu, Impact of environmental conditions on the sorption behavior of Pb(II) in Na-bentonite suspensions, *J. Hazard. Mater.* 183 (2010) 632–640, <https://doi.org/10.1016/j.jhazmat.2010.07.072>.
- [32] X. Miao, X. Yue, Z. Ji, X. Shen, H. Zhou, M. Liu, K. Xu, J. Zhu, G. Zhu, L. Kong, S. A. Shah, Nitrogen-doped carbon dots decorated on  $\text{g-C}_3\text{N}_4/\text{Ag}_3\text{PO}_4$  photocatalyst with improved visible light photocatalytic activity and mechanism insight, *Appl. Catal. B Environ.* 227 (2018) 459–469, <https://doi.org/10.1016/j.apcatb.2018.01.057>.
- [33] N. Nourieh, R. Nabizadeh, M.A. Faramarzi, S. Nasser, K. Yaghmaei, B. Mahmoudi, M. Alimohammadi, M. Khoobi, Photocatalytic degradation of ketoconazole by Z-scheme  $\text{Ag}_3\text{PO}_4/\text{graphene oxide}$ : response surface modeling and optimization, *Environ. Sci. Pollut. Res.* 27 (2020) 250–263, <https://doi.org/10.1007/s11356-019-06812-5>.
- [34] W. Zhang, L. Zhou, J. Shi, H. Deng, Synthesis of  $\text{Ag}_3\text{PO}_4/\text{G-C}_3\text{N}_4$  composite with enhanced photocatalytic performance for the photodegradation of diclofenac under visible light irradiation, *Catalysts* 8 (2) (2018) 45, <https://doi.org/10.3390/catal8020045>.
- [35] P. Sundarajan, P. Eswaran, A. Marimuthu, L.B. Subhadra, P. Kannaiyan, One pot synthesis and characterization of alginate stabilized semiconductor nanoparticles, *Bull. Korean Chem. Soc.* 33 (2012) 3218–3224, <https://doi.org/10.5012/bkcs.2012.33.10.3218>.
- [36] Z. Liu, Y. Liu, P. Xu, Z. Ma, J. Wang, H. Yuan, Rational design of wide spectral-responsive heterostructures of Au nanorod coupled  $\text{Ag}_3\text{PO}_4$  with enhanced photocatalytic performance, *ACS Appl. Mater. Interfaces* 9 (2017) 20620–20629, <https://doi.org/10.1021/acsami.7b06824>.
- [37] Q. Xie, Y. Li, Z. Lv, H. Zhou, X. Yang, J. Chen, H. Guo, Effective adsorption and removal of phosphate from aqueous solutions and eutrophic water by Fe-based MOFs of MIL-101, *Sci. Rep.* 7 (2017) 3316, <https://doi.org/10.1038/s41598-017-03526-x>.
- [38] R. Chong, X. Cheng, B. Wang, D. Li, Z. Chang, L. Zhang, Enhanced photocatalytic activity of  $\text{Ag}_3\text{PO}_4$  for oxygen evolution and methylene blue degradation: effect of calcination temperature, *Int. J. Hydrog. Energy* 41 (2016) 2575–2582, <https://doi.org/10.1016/j.ijhydene.2015.12.061>.
- [39] O. Pop-Georgievski, D. Kubies, J. Zemek, N. Neykova, R. Demianchuk, E. M. Chánová, M. Slouf, M. Houska, F. Rypáček, Self-assembled anchor layers/polysaccharide coatings on titanium surfaces: a study of functionalization and stability, *Beilstein J. Nanotechnol.* 6 (2015) 617–631, <https://doi.org/10.3762/bjnano.6.63>.
- [40] L. Luo, Y. Li, J. Hou, Y. Yang, Visible photocatalysis and photostability of  $\text{Ag}_3\text{PO}_4$  photocatalyst, *Appl. Surf. Sci.* 319 (2014) 332–338, <https://doi.org/10.1016/j.apsusc.2014.04.154>.
- [41] C. Pan, Y. Zhu, New type of  $\text{BiPO}_4$  oxy-acid salt photocatalyst with high photocatalytic activity on degradation of dye, *Environ. Sci. Technol.* 44 (2010) 5570–5574, <https://doi.org/10.1021/es101223n>.



# Surface modification of Ag<sub>3</sub>PO<sub>4</sub> using the alginate for highly active photocatalyst under visible light irradiation

## ORIGINALITY REPORT

7%

SIMILARITY INDEX

4%

INTERNET SOURCES

6%

PUBLICATIONS

1%

STUDENT PAPERS

## PRIMARY SOURCES

1

[ejournal2.undip.ac.id](http://ejournal2.undip.ac.id)

Internet Source

2%

2

Uyi Sulaeman, Richo Dwi Permadi, Dian Riana Ningsih, Hartiwi Diastuti, Anung Riapanitra, Shu Yin. "The surface modification of Ag<sub>3</sub>PO<sub>4</sub> using anionic platinum complexes for enhanced visible-light photocatalytic activity", Materials Letters, 2020

Publication

1%

3

Uyi Sulaeman, Dadan Hermawan, Roy Andreas, Ahmad Zuhairi Abdullah, Shu Yin. "Native defects in silver orthophosphate and their effects on photocatalytic activity under visible light irradiation", Applied Surface Science, 2018

Publication

1%

4

Uyi Sulaeman, Richo Dwi Permadi, Dian Riana Ningsih, Hartiwi Diastuti, Anung Riapanitra, Shu Yin. "Data of XPS in incorporating the

1%

# platinum complexes dopant on the surface of Ag<sub>3</sub>PO<sub>4</sub> photocatalyst", Data in Brief, 2020

Publication

5

Uyi Sulaeman, Suhendar Suhendar, Hartiwi Diastuti, Anung Riapanitra, Shu Yin. "Design of Ag<sub>3</sub>PO<sub>4</sub> for highly enhanced photocatalyst using hydroxyapatite as a source of phosphate ion", Solid State Sciences, 2018

Publication

1 %

6

Sci-Hub.se

Internet Source

1 %

7

Uyi Sulaeman, Estri Yunari, Ponco Iswanto, Shu Yin, Tsugio Sato. "Synthesis of Bi<sub>2</sub>O<sub>3</sub>/Ag<sub>3</sub>PO<sub>4</sub> Composites and their Photocatalytic Activities under Visible Light Irradiation", Advanced Materials Research, 2015

Publication

1 %

Exclude quotes

Off

Exclude matches

< 1%

Exclude bibliography

On